Influence of the supersaturated silicon solid solution concentration on the effectiveness of severe plastic deformation processing in Al-7wt%Si casting alloy

C.M. Cepeda-Jiménez[a], J.M. García-Infanta[a], A.P. Zhilyaev[a,b], O.A. Ruano[a], F. Carreño[a]

[a]*Department of Physical Metallurgy, CENIM, CSIC, Av. Gregorio del Amo 8, 28040 Madrid, Spain*

[b]*Institute for Metals Superplasticity Problems, Russian Academy of Science, 39 Khalturina, 450001 Ufa, Russia*

Abstract

A comparative study of room temperature severe plastic deformation (SPD) of a hypoeutectic Al–7wt% Si casting alloy by high pressure torsion (HPT) and equal channel angular pressing (ECAP) has been performed. Microstructural parameters and microhardness were evaluated in the present work. Three different initial Si solid solution contents have been considered: as cast (C sample, 1.6 wt% Si), annealed and quenched (Q sample, 1.2 wt% Si) and annealed and furnace cooled (S sample, 0.7 wt% Si). The samples processed by ECAP have smaller average Si particle sizes (0.9-1.7 μm), than those for samples processed by HPT (2.4-4.4 μm). The initial supersaturated Si solid solution is the major factor affecting the microstructure and the mechanical properties of the material. Fine deformation-induced Si precipitates from the supersaturated solid solution were responsible of the large grain refinement obtained by both SPD processing methods, which was considerably higher than that reported for pure aluminium. Q samples, processed by both SPD methods, containing an intermediate concentration of Si in solid solution, show the highest hardness due to the finest and most homogeneous microstructure. The finest and homogeneous grain size was ~0.2 μm for the HPTed and ~0.4 μm for the ECAPed, Q samples.

Keywords: B. Al-Si alloys; C. Severe plastic deformation (SPD);D. Deformation-induced precipitation; D. Microstructure; D. Mechanical properties.

*Corresponding author. Tel.: +34 91 5538900 ext.217; fax: +34 91 5347425.

E-mail address: cm.cepeda@cenim.csic.es (C.M. Cepeda-Jiménez)

1. Introduction

Hypoeutectic Al-Si alloys are widely used for castings in industry, especially in the automobile industry, because of their good mechanical properties at elevated

temperature, excellent wear resistance and low coefficient of expansion. However, one of the drawbacks is its low fracture toughness due to its microstructure, which consists of a primary aluminium phase, and an eutectic silicon second-phase present between the aluminium dendrites. Eutectic silicon crystals have complex shapes and most of these are three-dimensionally connected to each other, allowing the crack to advance readily along the brittle silicon crystals [1-5].

The homogenization and refinement of microstructure by deformation processing is beneficial to improve the mechanical properties of engineering materials [6]. Processing through the imposition of severe plastic deformation (SPD) provides the potential for significantly affecting the sizes and distributions of any second-phase particles and precipitates contained within the aluminium matrix [7-9], and additionally, to achieve grain refinement to the submicrometer or even the nanometer level [10]. The main feature of all SPD methods is the accumulation of large plastic strain without any remarkable change in the sample dimensions [11].

Although there are several different SPD processing procedures, most attention is currently directed to the processings of Equal-Channel Angular Pressing (ECAP) [12] and High-Pressure Torsion (HPT) [13].

In an idealized description of ECAP, deformation takes place by simple shear confined to a narrow zone at the plane of intersection of the die channels [6]. On the other hand, processing by HPT involves the application of a pressure, P, followed by torsional straining through the rotation of the lower anvil through a selected number of rotations. Surface frictional forces, therefore, deform the disk by shear so that deformation proceeds under a quasi-hydrostatic pressure [14].

Whereas ECAP is capable of producing relatively large bulk samples, HPT is used for small samples, generally in the form of disks, and it is ideal for processing hard materials because of the presence of a large hydrostatic pressure. Experiments show that the grain sizes achieved in HPT are generally smaller than those produced using ECAP [15].

Additionally, in aluminium alloys, microstructure refinement during SPD is strongly dependent on the strain path, and also on the introduction of second-phase particles to hinder boundary migration [16], or the use of solute to inhibit recovery [17,18]. Furthermore, dynamic processes such as solute precipitation [19-21] or dissolution [22] may occur during large plastic deformation, and they may influence the extent and nature of microstructure refinement.

Most investigations of SPD have considered pure metals and solid solution alloys, and strain-path effects in multi-phase alloys have received limited attention [2,3,8,20,21].

In the present work, the influence of the initial Si concentration in supersaturated solid solution of a hypoeutectic Al–Si alloy, on the microstructure refinement and strengthening obtained by two SPD processings, such as ECAP and HPT, has been investigated. Annealing at 540 ºC for 20 h, followed either by quenching or slow cooling prior to the SPD processing has been employed to control and reduce this supersaturated Si concentration.

The increase in Vickers microhardness achieved after processing has been analyzed in terms of deformation-induced precipitation from the supersaturated solid solution, grain refinement and homogenization of Si particle distribution. The role of the strain path considered, ECAP or HPT processing, in each of these processes, has been examined.

2. Experimental procedure

Pure Al (99.99 wt%) and an Al–12.3 wt% Si–0.02 wt% Na alloy were melted and casted into a mould to produce an ingot having dimensions of 400 mm × 250 mm × 40 mm. Emission spectroscopy of the resulting material revealed a composition (in wt%) of 7.0% Si, 0.3% Fe and balance Al. Samples processed in the as-cast condition are named C samples. Other samples were subjected to two different heat treatment sequences prior to SPD processing to control and reduce the supersaturated Si concentration in the as-cast C material: (a) annealing at 540 ºC for 20 h, followed by water quenching to room temperature (named as Q samples); and (b) annealing at 540 ºC for 20 h followed by slow cooling inside the furnace over 13.5 h (named as S samples). The three sets of samples were then subjected to severe plastic deformation by ECAP or HPT at room temperature.

ECAP billets with dimensions 90 mm × 10 mm × 10 mm were machined along the largest dimension of the as-cast ingot. ECAP processing was performed at room temperature using a sharp-cornered 90º ECAP die (zero die-relief angle at the outer corner of the die channel intersection), at a pressing speed of 10 mm/min. Each sample was pressed repetitively through a total of four passes, equivalent to imposed strains of ~4, with the samples rotated 90° in the same sense between each pass, i.e. by route B_C.

It has been shown experimentally that optimum ECAP processing for homogeneous materials is achieved using route B_C, because this leads to an array of equiaxed grains separated by high misorientation angles [23]. In this study, the route B_C was selected due to its redundant nature that does not modify the initial dendritic structure of the Al-7 wt% Si alloy. Thus, the influence of solid solution concentration in the aluminium matrix can be studied without the interference effect of eutectic particles redistribution produced by other routes.

Additionally, disk samples for HPT were machined with dimensions ~1 mm thick and 10 mm in diameter. HPT processing was carried out through five whole revolutions at room temperature at 1 rpm, which corresponds to five minutes of processing. The applied pressure was 6 GPa and a constrained HPT facility was employed [24,25]. Details on the principles of HPT were given earlier [26]. The final thickness of the HPT samples was ~0.65 mm.

Processed samples were characterized using both optical and scanning electron microscopes, and microhardness measurements. ECAPed samples were always examined at the middle of the ECAP flow plane, in order to avoid die wall effects. On the other hand, HPTed samples were characterized on the top surfaces of the HPT disks on the periphery disc zone (~0.8 r).

Metallographic observation involved methods of standard surface preparation. The samples were mechanically polished, and then electropolished in a 30% nitric acid solution in methanol at -28 ºC and 17 V. The microstructure was observed by scanning electron microscopy (SEM) using a JEOL JSM 6500F equipment with field emission gun. Energy-dispersive X-ray spectroscopy (EDX) analysis to identify the concentration of silicon within the aluminium dendrites and the different phases present in the Al-7 wt% Si alloy was performed by an electron probe microanalyzer (Oxford Inca) operating at 15 kV.

Grain size was measured on the primary Al constituent, for all the processed conditions, from SEM images obtained using backscattered electrons. The mean linear intercept method was employed, without discriminating between high- and low-angle boundaries. Eutectic Si particles were analyzed by optical microscopy. Optical and scanning electron micrographs were analyzed using the Sigma Scan Pro software in order to obtain the size distribution of the Si precipitates, and aluminium matrix grains. Because the particles were not spherical in the alloy, the maximum dimension of the particle was used as the particle size. More than 550 precipitates and 200 grains for each thermal condition were analyzed. Particles and grain size data fell into log-normal distributions, so the geometric mean value was chosen as a measure of the size.

Vickers microhardness was measured on the flow plane of ECAPed samples and along the diameter of processed HPT disks, using a Matsuzawa Seiki MHT-1 microhardness tester. Loads of 1 kg during 15 s, both for the un-processed samples and severely deformed materials, were applied. Additionally, for ECAPed samples smaller indentations using loads of 10 g were made, taking care to imprint in the centre of the primary Al dendrites.

3. Results

3.1. Materials

Fig. 1 shows the phase diagram of the Al–Si system [27]. The eutectic is formed between an aluminium solid solution containing only 1.65 wt% silicon (at the eutectic temperature, about 577 ºC), and virtually pure silicon as the second phase. EDX measurements (Table 1) reveal that for the as-received material, i.e the as-cast material referenced as C sample, 1.6 wt% Si is retained in supersaturated solid solution within the middle of primary Al dendritic cells. Additionally, in this study, annealing at 540 ºC for 20 h followed either by quenching (Q sample) or slow cooling (S sample) has been employed to control and reduce this supersaturated Si concentration. According to the phase diagram (Fig. 1), Si solubility at 540 ºC amounts 1.2 wt%. The EDX measurements confirm 1.1 ± 0.2 wt% Si for the annealed and quenched Q sample, and 0.7 ± 0.1 wt% Si for the furnace cooled S sample.

3.2. Microstructure

Fig. 2 shows optical micrographs at two magnifications of the primary Al dendritic cells and the Si particle distribution in the as-cast alloy (C sample), and after thermal treatments to modify the solid solution in the Al matrix (Q and S samples). The microstructure of the Na-modified Al–7 wt.% Si in the as-cast C sample (Fig. 2a-b) consists of large grains, including the primary Al dendrites, which are surrounded by the interdendritic network of eutectic constituent, which contains a distribution of mainly irregular Si fibres, and a small volume fraction of needle-like Al_5FeSi phase, consequence of Fe impurities on the alloy. The primary Al dendrite cell size varies from 25 to 65 μm, due to the difference in solidification rates at different locations in the as-cast ingot. After annealing at 540 ºC for 20 h (Fig. 2c to f), coarsening and slight spheroidization of the silicon particles occurs. An eventual disappearance of small Si particles inside the eutectic region is observed in comparison with Figs. 2a and b.

Fig. 3 shows optical micrographs of the Si particles distribution for the C sample produced after 4 (Fig. 3a) or 8 (Fig. 3b) ECAP-B_C passes, and after HPT processing (Fig. 3c-d). Fig. 3c corresponds to an optical micrograph on the central HPT disk zone, and Fig. 3d on the periphery disk zone. Each processing route leads to different distribution of the eutectic silicon particles. After processing by ECAP-route B_C the microstructure after four passes (Fig. 3a) or eight passes (Fig. 3b) consists of quasi-equiaxed primary Al dendritic cells, being similar in size to those in the as-cast material. Essentially, no homogenization of the particle geometrical distribution is apparent for this redundant straining, and every four passes by this route B_C, the macrostructures closely resemble that of the as-cast condition.

On the other hand, by HPT processing, the initial compression together with the progressive shearing of the primary Al dendrites causes their size to be continuously

reduced, and a homogenous Si particle distribution in the Al matrix approximately 1 mm from the disk centre to the edge of the HPT disk is observed (Fig. 3d). Additionally, it is apparent from Fig. 3c that for the central disk zone, the Si particles are not distributed homogeneously and they follow the flow of the torsional straining. This development of swirls and vortices in the centre of the disc also has been observed in other HPT processed materials, such as pure Al [28,29], Cu-Ag alloy [30], Mg AZ31 alloy [31], pearlitic steel [32] and an austenite/ferrite duplex stainless steel [33].

The dissimilarities between the Si particle geometrical distributions after severe plastic deformation reflect the difference in deformation path by HPT processing, with monotonic shearing, in comparison to ECAP by route B_C, with redundant straining.

Fig. 4 shows optical micrographs of the Si particles for the different supersaturated Si solid solution conditions (C, Q, and S samples) after 4 ECAP-B_C passes (Fig. 4a-c), and HPT processing (Fig. 4d-f) at the periphery of the HPT disks.

It is apparent from a comparison of Fig. 4a (ECAPed C sample) and Fig. 4d (HPTed C sample), with Fig. 2b (as-cast C sample), that the rod-shaped particles visible in the as-cast C sample are no longer present, and they have been replaced by more equiaxed particles. These observations demonstrate that in both processing methods, ECAP and HPT, the high pressures imposed together with the shear stresses developed during straining lead to fragmentation of the largest particles.

However, the average particle size clearly is larger for the HPTed C sample, in contrast with the ECAPed C sample. This indicates an initial fragmentation of the three dimensional network of silicon fibres during both processing methods, followed by substantial coarsening during HPT processing.

Additionally, for the HPTed Q and S samples (Fig. 4e-f), the Si particle morphology coarsened slightly in comparison with the un-processed samples (Fig. 2d,f). By contrast, for the ECAPed Q and S samples (Fig. 4b-c), eutectic silicon particles become smaller in size in comparison with the un-processed samples, indicating that they were broken more extensively during ECAP processing than by HPT processing.

The average particle size for ECAPed C, Q and S samples after 4 passes through B_C route was 0.95, 1.7 and 1.4 μm respectively. The average Si particle size for ECAPed Q and S samples can be considered almost the same, and the small difference in particle size should be attributed to the heterogeneity in the initial casting alloy, and to experimental scatter in their determination due to the irregular shape. On the other hand, the average size values for HPTed C, Q and S samples were 2.4, 4.3 and 4.4 μm, respectively. It appears, therefore, that the stresses imposed by ECAP are more effective in breaking Si particles. This claim will be discussed later.

Fig. 5 shows the matrix microstructure for the processed C samples after 4 ECAP passes (Fig. 5a-b), and after HPT processing at the periphery of the disks (Fig. 5c-d). Secondary electron (SE) micrographs (Fig. 5a,c), and crystallographic contrast images using backscattered electrons (BSE) (Fig. 5b,d) were obtained. For HPTed samples no visible difference was found in the Al matrix microstructure between the centre and in the periphery disk, according with previous results where similar torsional strain was imposed [25].

From inspection of the BSE micrographs in Fig. 5b and d, it is immediately apparent that substantial grain refinement has been achieved using both processing procedures. Average values of grain/subgrain size measured from such images are summarized in Table 2.

Fig. 5a and b, corresponding to ECAPed C samples, shows that ECAP produces a shear band structure, which is clearly distinguishable after 4 passes. Additionally, an array of ultrafine (sub)grains are observed within the shear band structure, which are almost equiaxed, although in some areas are slightly elongated. Furthermore, the (sub)grain boundaries are not well defined and the contrast within the grains is non-uniform, which is indicative of a work hardened structure. The mean (sub)grain size was estimated as ~0.3 μm after ECAP straining (Table 2).

On the other hand, for the HPTed C sample two zones, delineated by a broken line, with different grain size are clearly observed (~0.2 and 0.5 μm). In both zones, the Al matrix grains were equiaxed with better-defined grain boundaries than for ECAPed C sample. This is consistent with the higher imposed straining during HPT processing, which can favour recovery and/or recrystallization during or after the processing, due to the high introduced energy in the severely deformed material.

In addition, by secondary electron images (Fig. 5a and c), it can be observed for both SPD processings the precipitation of small Si particles (<100 nm in size) within the aluminium matrix. Inspection of the primary Al dendrite cells for the un-processed C sample, and thermal treated Q and S samples, using both SE and BSE modes, did not reveal these small precipitates in the Al matrix. The absence of these small precipitates in the as-cast unprocessed samples corroborates that precipitation is induced by deformation, and takes place during the severe plastic deformation or immediately after the processing [20,21]. Furthermore, the small Si precipitates appear to be distributed along the grain boundaries and aligned with the shear bands structure in the ECAPed C sample (Fig. 5a), and more homogeneously distributed for HPTed C sample (Fig. 5c). Additionally, for the HPTed C sample, there was clear evidence for small precipitates-free zones near a high fraction of the large eutectic Si particles. Within these zones, there was a larger grain size in the aluminium matrix (Fig. 5d). Thus, the presence of

fine Si precipitates should be the main reason why the grain size is smaller where this precipitates are present. This also explains the region of larger grain size, where these small precipitates were not observed.

Fig. 6 shows secondary and backscattered electron micrographs for the ECAPed Q sample (Fig. 6a-b), and the HPTed Q sample (Fig. 6c-d), where again a clear difference between the microstructures obtained by both processing methods is observed. For ECAPed Q sample (Fig. 6a-b), deformation processing leads to the creation of a slightly elongated deformation substructure oriented closely with the shear direction of the fourth pass. In comparison with ECAPed C sample (Fig. 5b), the (sub)grain microstructure is better contrasted and defined, although the average size is slightly larger, being ~0.4 μm (Table 2). Similarly to ECAPed C sample, deformation-induced Si precipitates appear decorating grain boundaries that in the early stages of ECAP straining delimitated shear bands.

On the other hand, high number of nanometric Si precipitates induced by deformation and homogenously distributed can be observed in the HPTed Q sample (Fig. 6c). The corresponding BSE micrograph in Fig. 6d reveals the presence of an array of fine grains, with an average grain size of ~200 nm. This grain size for the HPTed Q sample is similar to that for the HPTed C sample in the UFG region (Fig. 5d).

Fig. 7 shows similar electron micrographs composition as Fig. 6, but it corresponds to processed S samples. In general, in comparison with processed Q samples, the average (sub)grain size is coarser (Table 2), being ~0.8 μm for the ECAPed S sample (Fig. 7a and b), and ~0.4 μm for the HPTed S sample (Fig. 7c and d). The microstructure for both S processed samples is well-defined and rather homogenous, and, in comparison with processed Q samples, smaller number of nanometric Si precipitates induced by deformation are observed.

Finally, Fig. 8 includes BSE micrographs, showing the grain microstructure of the aluminium matrix surrounding coarse Si particles. Fig. 8a corresponds to HPTed C sample, Fig. 8b to HPTed Q sample and finally Fig. 8c to HPTed S sample. Similar analysis could not be performed in the ECAPed samples due to the high concentration of non-conducting Si particles in the interdendritic zone, which make difficult to set the SEM microscopy conditions to reveal the microstructure around them. In general, the microstructure for HPTed S and Q samples is essentially equiaxed in grain size and there is no evidence for the presence of any region with a coarsened structure, even close to the large eutectic Si particles. However, the microstructure corresponding to the HPTed C samples (Fig. 8a) shows, as in Fig. 5d, coarsened grains of heterogeneous size close to the large eutectic Si particles. Thus, the microstructure in the HPTed C sample is not as homogeneous as for the thermal treated HPT processed samples (Q and S).

3.3. Microhardness test

The values of the Vickers microhardness, HV, were measured on the flow plane for the ECAPed samples and across the diameter of the disk for HPTed samples, and the results are summarized in Table 3. HV values for the as-cast Al-7wt%Si samples subjected to the different thermal treatments have also been included for comparison. Large indentation imprints with 1 kg load were carried out to measure the contribution of the aluminium matrix and the eutectic Si particles in the un-processed and processed samples. Additionally, smaller imprints using loads of 10 g during 15 s for the ECAPed samples were intentionally carried out inside of the primary Al dendrites, far away from the eutectic Si particles.

It is worth noting that the HV values remain practically constant across all of the HPT disks. The trend of the constant hardness with the distance suggests that there was a gradual development into a reasonably homogeneous microstructure [34].

The microhardness value for the sample in the undeformed initial state is slightly higher for the C sample (44 HV), followed by the value for the Q sample (42 HV), and finally the S sample (34 HV). The microhardness decrease after thermal treatment at 540 ºC for 20 h is caused by relaxation of residual stresses and loss of solute content defined by the phase diagram (Fig. 1), which effectively reduces the number of obstacles available to impede the dislocation movement leading therefore to an inherent softening of the material.

The hardness increases significantly for all processed samples, although clear differences are apparent for both processings and indentation loads considered.

In general, samples containing similar supersaturated Si solid solution present higher strength if they are processed by HPT, than those processed by ECAP. This can be attributed to the fact that the first one produces more homogenous deformation-induced precipitation, and thus, finer (sub)grain microstructure.

Additionally, similar trend for both processings is observed when 1 kg load was applied. The material annealed and quenched followed by SPD processing (Q sample) exhibited the highest hardness, being 84 HV after HPT processing, and 73 HV after ECAP processing. The microhardness values for the as-cast HPTed material (C sample) were, a priori unexpectedly, between those of the processed Q and S samples. However, when small indentations (10 g in load) were carried out inside the aluminium dendrite for ECAPed samples (Table 3), the highest HV value was obtained for the ECAPed C sample, 72 HV, followed by Q and S samples respectively.

Therefore, two different trends are observed regarding the use of low and high loads in the Vickers microhardness tests, which will be discussed in the next section.

4. Discussion

In the present study, severe plastic deformation was imposed on a hypoeutectic Al-7 wt% Si alloy using both ECAP and HPT processings. Additionally, annealing at 540 ºC for 20 h prior to both processing methods was performed to control and reduce the supersaturated Si concentration in the as-cast material for studying its influence on the processing effectiveness, regarding to grain refining and microhardness increase.

After the thermal treatment, the initial content of supersaturated Si solid solution in the primary Al in the as-cast material (C samples) decreased from ~1.6 wt% to ~1.1 wt% Si for the annealed and quenched Q sample, and to ~0.7 wt% Si for the annealed and slow cooled S sample (Table 1).

The results of this study demonstrate that both the Si solid solution content and the processing path determine the microstructure (Fig. 3-8) and the Vickers microhardness (Table 3) obtained after processing. These findings do not agree with previous studies where the thermo-mechanical condition of a sample prior to HPT had relatively little effect on the subsequent mechanical properties after processing [10].

4.1. Supersaturated silicon solid solution and grain refining

For both SPD processing methods considered in the present research, substantial refinement in grain size was observed (Table 2), being this in general higher for HPTed samples than for ECAPed samples [26,35]. However, in this study the difference in grain size for both processing methods, for the C sample, is mainly attributed to the amount of Si solid solution and, secondarily, to the severity of the forming process. In addition, Table 2 reveals that decreasing amount of initial solid solution corresponds to an increase of grain size. Furthermore, differences in grain refining between both processing methods is increased for the processed S sample, which in contrast contains the lowest initial Si solid solution content. As described, there is enough evidence of the great importance of the deformation-induced Si precipitation from the supersaturated solid solution in determining the grain size.

From the BSE micrographs included in Fig. 5-7, it is readily apparent that processing by ECAP-B_C and HPT involve different deformation paths, which lead to different grain morphology and refinement degree (Table 2). It has been reported [36] that processing by ECAP-B_C leads to grain refinement and HAB generation through internal subdivision. The Al-7 wt% Si alloy developed deformation bands (DBs) upon deformation through the ECAP shear zone, which with increasing strain developed grain sub-division. This is in general agreement to earlier findings [6,37]. In contrast, processing by HPT involves the progressive elongation of the primary Al dendrite cells, and HABs may be generated by geometric-dynamic recrystallization, as well as by

processes of grain subdivision. In general, for HPT samples, the grain boundaries are well defined and the overall appearance is consistent with a low-energy microstructure after significant recovery.

On the other hand, the grain sizes were much smaller than 1.3 μm reported for pure aluminium after 4 passes of ECAP [38], or 1.2 μm after 5 turns of HPT under a pressure of 6 GPa [39]. This is further evidence that deformation-induced precipitation of nanometric precipitates from the available Si solid solution is the main responsible of the extra refinement achieved during SPD processing.

Accordingly, severe plastic deformation carried out on the annealed and slow cooled S samples containing the lowest initial Si solute concentration leads to coarser grain size (Fig. 7) than that for C or Q samples with higher amount of deformation-induced precipitates (Fig. 5 and 6). Such smaller number of precipitates produces a smaller pinning/dragging effect on the dislocations and boundaries, such that more extensive dislocation recovery and grain growth can occur.

For ECAP processed samples, fine Si precipitates were observed predominantly within grain boundaries delineating shear bands. In contrast, for HPT processed samples, Si precipitates were more homogeneously distributed through the aluminium matrix. This location of Si precipitation as a function of the straining path determines the final (sub)grain size, which was smaller for HPT processed samples. However, the location of Si particles as a function of the processing is unresolved, and it requires more research on the microstructural development from the earliest stages of deformation for both processings.

Additionally, whereas the annealed and processed Q and S samples with lower initial solid solution content showed uniform grain size (Fig. 6-8), the HPTed C sample with the highest initial Si solid solution showed a bimodal microstructure (Fig. 5 and 8). This microstructure consisted of UFG regions (~200 nm) where deformation-induced precipitation of fine Si particles was clearly observed (Fig. 5), and zones with coarsened grains (~0.5 μm) adjacent to the large eutectic Si particles, where deformation-induced precipitates were not present. As mentioned previously, this bimodal microstructure could not be observed in ECAP processed C sample. However, it is our contention that close to the interdendritic silicon particles in the ECAPed C sample, some areas with coarsened grains and depleted solid solution will be also present.

Accordingly, the main factor to explain the heterogeneous microstructure for the processed as-cast C samples, which leads to a lower hardness than expected for both SPD processing methods (Table 3), is the non-equilibrium state of the as-cast C sample due to the fast solidification during the casting process. The high and heterogeneous solid solution supersaturation after the cast processing increases the chemical driving

force for bulk diffusion of Si from the solid solution to the eutectic Si particles, creating areas around these particles depleted of solid solution. Additionally, together with the non-equilibrium state and the highest supersaturated solid solution, severe plastic deformation by HPT processing produces higher dislocation density, especially near large eutectic Si particles, due to large local strain gradients. The Si diffuses assisted by dislocations to the eutectic Si particles, leaving solute free zones. Thus, the decrease in pinning effect by small precipitates, together with dynamic recovery assisted by the high dislocation density close to these large Si particles leads to a coarse-grained aluminium matrix near these particles [40,41]. The effect of supplying solute by dislocation pipe diffusion to the eutectic Si particles diminishes as recovery occurs [42]. Therefore, ultrafine grains were still observed in zones where Si solid solution was enough to induce precipitation of fine Si particles, thus obtaining the bimodal microstructure previously mentioned. For the ECAPed C sample, the microstructure could be observed only in the dendrite centre where less Si diffusion occurred. Accordingly, only fine grains are observed.

On the contrary, the prolonged annealing at 540 ºC for 20 h prior to SPD processing methods to control the supersaturated Si content (Q and S samples), leads to an equilibrium state, accordingly to the phase diagram (Fig. 1). Therefore, no concentration gradient and no chemical driving force for Si diffusion exist. Thus, substantial additional Si diffusion during SPD does not occur, and a homogeneous distribution of deformation-induced Si precipitates and grain sizes is obtained (Fig. 8).

4.2. Deformation path and eutectic silicon particles.

It was clearly observed for the HPT processed C sample (Fig. 4d) that the eutectic Si and Al_5FeSi particles were broken during processing, and coarsened considerably in comparison with the as-cast C sample (Fig. 2b). However, this change in Si particle size is not as notable for the ECAPed C sample (Fig. 4a), taking into account the same starting non-equilibrium state. Thus, it is our contention that the Si particle coarsening for the HPTed C sample is due to the following factors: i) the initial non-equilibrium state, which accelerates diffusion from the supersaturated solid solution; ii) the relatively prolonged processing time (5 min) and the increase in temperature during HPT due to the high imposed strain which also favours diffusion; and iii) the homogenous redistribution of the eutectic Si particles in the Al matrix, which decreases the diffusion distance between particles. On the contrary, the redundant (non-redistributing) nature of the straining for ECAP-B_C processing [8,43], together with the shorter duration of straining, i.e. the time passing through the die channel intersection, which minimizes an increase of temperature, slow down the Si solid solution diffusion

from the centre of the primary Al dendrite cells to the eutectic constituent. This justifies the small change observed in the Si particles size (Fig. 4) for the ECAPed C sample.

On the other hand, for all processed samples considered, ECAP processing gave rise to finer average Si particle size (0.9-1.7 μm) than in HPT processing (2.4-4.4 μm). It is worth noting that ECAP processing is more effective in breaking Si particles. As mentioned previously, the annealing treatment performed prior to SPD processing (Q and S samples) leads to an equilibrium state, decreasing the driving force for Si diffusion. As shown in Fig. 2, the eutectic Si particles in the initial as-cast sample were considerably coarsened by the annealing treatment of the Q and S samples, reaching a quasi-equilibrium state, since their size and morphology was scarcely modified during the following HPT processing (Fig. 4e-f). This indicates that substantial additional Si diffusion during HPT processing is not taking place. A comparison of HPT with ECAPed Q and S samples (Fig. 4b-c), and assuming that additional Si diffusion is not occurring, corroborates that ECAP processing is more effective in fracturing Si particles. The higher effectiveness in breaking Si particles of ECAP processing in comparison with HPT processing is due to higher shear stress concentration on the samples, which are forced to pass through the intersection of the channels [44]. Furthermore, the redundant nature of the ECAP strain, which maintains the initial eutectic distribution, favours additional stress concentration on the particles. On the contrary, the high hydrostatic pressure during HPT processing, together with the more homogeneous redistribution of Si particles on the soft Al matrix and the mentioned temperature increase during processing favour the stress distribution on the sample, reducing the potential for crack nucleation and particle fracture.

4.3. Supersaturated silicon solid solution and Vickers microhardness.

Finally, Vickers microhardness results (Table 3) showed that whilst SPD processing increased hardness in all samples considered, the magnitude of this increase is mainly influenced by the deformation-induced precipitation from the available supersaturated Si solid solution concentration, which determines the grain size, and in a minor extent by the deformation path.

It is our contention that not residual solid solution is present after SPD processing, thus, not contributing to hardness. The absence of these small precipitates in the as-cast unprocessed samples corroborates that precipitation is induced by deformation, and takes place during or immediately after SPD processing. Furthermore, the amount of these deformation-induced precipitates increases with the initial solid solution concentration, suggesting that this is consumed during deformation.

On the other hand, the contribution of dislocation density to hardness values is not taken into account, since the high stacking fault energy (SFE) for aluminium leads to rapid recovery rates, especially when high deformations are imposed during SPD processing. In general, for all processed samples well-defined grains were observed by backscattered electron micrographs, suggesting that recovery and/or recrystallization processes have taken place, and dislocation density must be similar for all processed samples.

Prior to SPD, as-cast Al-7 wt% Si alloy and thermal treated samples have low hardness (~34-44 HV), and the slight differences between the samples are predominantly due to solid solution strengthening, according to the expected trend ($HV_C > HV_Q > HV_S$).

After SPD processing, the microstructural differences between C, Q and S processed samples are reflected in the hardness of the different samples. However, the new size and distribution of the large eutectic Si particles after SPD processing does not become important for significant hardening, because they remain coarse and widely separated. When loads of 1 kg were considered to carry out the microhardness test, a similar trend for both SPD processing was obtained, being well correlated with the (sub)grain size observed. Accordingly, processing of the sample with the lowest initial Si solid solution concentration (S) leads to larger grain size than those for the more supersaturated ones (C and Q), and the lowest HV values were obtained, being 51 HV for the ECAPed S sample and 64 HV for the HPTed S sample. On the other hand, the processed Q samples have shown the highest hardness, due to the finest and homogenous microstructure across the processed samples. In contrast, processed C samples, initially containing the highest concentration of solid solution, showed less hardness than those for processed Q samples by both SPD processing methods. This a priori unexpected result for processed C samples is attributed to a combination of hardening by UFG refining and deformation-induced precipitation, and softening due to loss of solute content close to the large Si particles together with recovery of the deformation structure, clearly observed for the HPTed C sample. This is thought to occur also for the ECAPed C sample, although at a lesser extent than for the HPTed C sample, because the same trend in HV values is observed. This suggests a similar bimodal microstructure around the eutectic constituent. However, the lower difference between HV values for ECAPed Q and C samples (73 and 69 HV, respectively), than that for HPTed Q and C samples (84 and 77 HV, respectively) corroborates the existence of less Si diffusion from the centre of the dendrites to the eutectic constituent, and thus less microstructural heterogeneity for the ECAPed C sample. This is completely confirmed when small imprints of 10 g load are performed in the centre of

the dendrites. In this test the possible softening by contribution of coarsened microstructure close to the eutectic Si particles due to solute depletion is avoided, obtaining the expected trend in microhardness values as a function of the initial supersaturated solid solution, i.e. $HV_C > HV_Q > HV_S$.

In summary, the results presented in this study demonstrate that small variations in initial Si solid solution content lead to different effects of the SPD processing methods on the microstructure and microhardness of the Al-7 wt% Si alloy.

5. Conclusions

Three different samples of Al-7 wt% Si subjected to thermal treatments to control the supersaturated Si concentration were processed by two SPD methods: equal-channel angular pressing (ECAP) and high-pressure torsion (HPT). The initial Si concentrations considered were: as cast (C sample-1.6 wt%), annealed and quenched (Q sample-1.1 wt%) and annealed and furnace cooled (S sample-0.7 wt%).The main conclusions of this study are as follows:

1. The initial Si solid solution concentration is the major factor affecting the microstructure and the mechanical properties of the processed material.
2. The grain sizes obtained for both processing methods were much smaller than reported for pure aluminium due to deformation-induced precipitation of small Si precipitates from the supersaturated solid solution.
3. For similar initial Si solid solution content, the grain refining and the hardness increase were higher for HPTed samples than those for the corresponding ECAPed samples. This is due to the fact that HPT produces more homogeneous deformation-induced precipitates distribution than ECAP processing, where precipitates appear decorating grain boundaries and aligned with shear bands.
4. SPD processed Q samples, containing the intermediate initial content of supersaturated Si solid solution (1.1 wt% Si), have shown the finest and the most homogeneous microstructure across the processed samples, being the grain size ~0.2 μm for the HPTed Q sample and ~0.4 μm for the ECAPed Q sample. Furthermore, the processed Q samples also showed the highest hardness in comparison with processed C and S samples.
5. Processed as-cast C samples showed lower microhardness values than expected due to their heterogeneous microstructure. The non-equilibrium state of the initial as-cast C sample promotes diffusion of Si solute to the eutectic particles, creating areas around these particles depleted of solid solution and, thus, with coarsened grain sizes.

6. For all processed samples, ECAP processing produced smaller average Si particle size (0.9-1.7 μm), than that for HPT processed samples (2.4-4.4 μm).

Acknowledgements

Financial support from MICINN (Project MAT2009-14452) is gratefully acknowledged. A.P. Zhilyaev thanks the Spanish Ministry of Science and Innovation for a Ramón y Cajal contract.

References

1. M.J. Starink, A.-M- Zahra, Mater. Sci. Eng. A 241 (1998) 277-280.

2. A. Ma, M. Takagi, N. Saito, H. Iwata, Y. Nishida, K. Suzuki, I. Shigematsu, Mater. Sci. Eng. A 408 (2005) 147-153.

3. J.M. García-Infanta, A.P. Zhilyaev, C.M. Cepeda-Jiménez, O.A. Ruano, F. Carreño, Scripta Mater. 58 (2008) 138-141.

4. T. Hosch, R.E.Napolitano, Mater. Sci. Eng. A 528 (2010) 226-232.

5. Q.G. Wang, M. Praud, A. Needleman, K.S. Kim, J.R. Griffiths, C.J. Davidson, C.H. Cáceres, A.A. Benzerga, Acta Mater. 58 (2010) 3006-3013.

6. A.P. Zhilyaev, D.L. Swisher, K. Oh-ishi, T.G. Langdon, T.R. McNelley, Mater. Sci. Eng. A 429 (2006) 137-148.

7. A.Ma, K. Suzuki, Y. Nishida, N. Saito, I. Shigematsu, M. Takagi, H. Iwata, A. Watazu, T. Imura, Acta Mater. 53 (2005) 211-220.

8. J.M. García-Infanta, S. Swaminathan, A.P. Zhilyaev, F. Carreño, O.A. Ruano, T.R. McNelley, Mater. Sci. Eng. A 485 (2008) 160-175.

9. M. Kawasaki, B. Ahn, T.G. Langdon, Acta Mater. 58 (2010) 919-930.

10. S.V. Dobatkin, E.N. Bastarache, G. Sakai, T. Fujita; Z. Horita, T.G. Langdon, Mater. Sci. Eng. A 408 (2005) 141-146.

11. R.Z. Valiev, R.K. Islamgaliev, I.V. Alexandrov, Progress Mater. Sci. 45 (2000) 103-189.

12. R.Z. Valiev, T.G. Langdon, Progress Mater. Sci. 51 (2006) 881-981.

13. A.P. Zhilyaev, T.G. Langdon, Progress Mater. Sci. 53 (2008) 893-979.

14. A.P. Zhilyaev, G.V. Nurislamova, B.-K. Kim, M.D. Baró, J.A. Szpunar, T.G. Langdon, Acta Mater. 51 (2003) 753-765.

15. A. Loucif, R.B. Figueiredo, T. Baudin, F. Brisset, T.G. Langdon, Mater. Sci. Eng. A 527 (2010) 4864-4869.

16. P.J. Apps, M. Berta, P.B. Prangnell, Acta Mater. 53 (2005) 499-511.

17. Y. Iwahashi, Z. Horita, M. Nemoto, T.G. Langdon, Metall. Mater. Trans. A 29 (1998) 2503-2510.
18. Y.H. Zhao, Y.T. Zhu, X.Z. Liao, Z. Horita, T.G. Langdon, Mater. Sci. Eng. A 463 (2007) 22-26.
19. H.W. Kim, S.B. Kang, N. Tsuji, Y. Minamino, Acta Mater. 53 (2005)1737-1749.
20. A.P. Zhilyaev, J.M. García-Infanta, F. Carreño, T.G. Langdon, O.A. Ruano, Scripta Mater. 57 (2007) 763-765.
21. J.M. García-Infanta, S. Swaminathan, C.M. Cepeda-Jiménez, T.R. McNelley, O.A. Ruano, F. Carreño, J. Alloy Compd. 478 (2009) 139-143.
22. A. Korchef, Y. Champion, N. Njah, J. Alloy Compd. 427 (2007) 176-182.
23. K. Oh-Ishi, Z. Horita, M. Furukawa, N. Nemoto, T.G. Langdon, Metall. Mater. Trans. A 29 (1998) 2011-2013.
24. A.P. Zhilyaev, S. Lee, G.V. Nurislamova, R.Z. Valiev, T.G. Langdon, Scripta Mater. 44 (2001) 2753-2758.
25. A.P. Zhilyaev, K. Oh-ishi, T.G. Langdon, T.R. McNelley, Mater. Sci. Eng. A 410-411 (2005) 277-280.
26. A.P. Zhilyaev, B.-K. Kim, J.A. Szpunar, M.D. Baró, T.G. Langdon, Mater. Sci. Eng. A 391 (2005) 377-389.
27. J.L. Murray, A.J. MacAlister, Bull. Alloy Phase Diagr. 5 (1984) 74-84.
28. G. Sakai, Z. Horita, T.G. Langdon, Mater. Sci. Eng. A 393 (2005) 344-351.
29. M. Kawasaki, T.G. Langdon, Mater. Sci. Eng. A 498 (2008) 341-348.
30. Y.Z. Tian, X.H. An, S.D. Wu, Z.F. Zhang, R.B. Figueiredo, N. Gao, T.G. Langdon, Scripta Mater. 63 (2010) 65-68
31. R.B. Figueiredo, T.G. Langdon, Mater. Sci. Eng. A 528 (2011) 4500-4506.
32. Y. Ivanisenko, W. Lojkowski, R.Z. Valiev, H.J. Fecht, Acta Mater. 51 (2003) 5555-5570.
33. Y. Cao, Y.B. Wang, R.B. Figueiredo, L. Chang, X.Z. Liao, M. Kawasaki, W.L. Zheng, S.P. Ringer, T.G. Langdon, Y.T. Zhu, Acta Mater (2011) *In press.*
34. C. Xu, Z. Horita, T. G. Langdon, Acta Mater. 56 (2008) 5168-5176.
35. A.P. Zhilyaev, B.-K. Kim, G.V. Nurislamova, M.D. Baró, J.A. Szpunar, T.G. Langdon, Scripta Mater. 46 (2002) 575-580.
36. Y. Huang, J.D. Robson, P.B. Prangnell, Acta Mater. 58 (2010) 1643-1657.
37. J. C. Werenskiold, H. J. Roven, Mater. Sci. Eng. A 410-411 (2005) 174-177.
38. Y. Iwahashi, Z. Horita, M. Nemoto, T.G. Langdon, Acta Mater. 46 (1998) 3317-3331.
39. C. Xu, Z. Horita, T.G. Langdon, Acta Mater. 55 (2007) 203-212.

40. J. Dennis, P.S. Bate, F.J. Humphreys, Acta Mater. 57 (2009) 4539-4547.
41. O.V. Rofman, P.S. Bate, Acta Mater. 58 (2010) 2527-2534.
42. Y. Huang, J.D. Robson, P.B. Prangnell, Acta Mater. 58 (2010) 1643-1657.
43. S. Swaminathan, J.M. García-Infanta, T.R. McNelley, O.A. Ruano, F. Carreño, J. Mater. Sci. 43 (2008) 7501-7506.
44. W.H. Hunt Jr., J.R. Brockenbrough, P.E. Magnusen, Scripta Metall. Mater. 25 (1991) 15-20.

Figure Captions

Fig. 1. Detail of the Al-Si phase diagram from 0 to 5 wt% Si.

Fig. 2. Optical micrographs at two magnifications showing primary Al dendritic cells and eutectic Si particles in the Al-7 wt% Si alloy subjected to different thermal treatments: a) and b) as-cast C sample; c) and d) annealed and quenched Q sample; e) and f) annealed and furnace cooled S sample.

Fig. 3. Optical micrographs of the as-cast Al-7 wt% Si alloy (C sample) processed by: a) 4 ECAP passes and b) 8 ECAP passes by route B_C; c) HPT-N=5 and 6 GPa on the central disc zone; and d) HPT-N=5 and 6 GPa on the periphery disc zone.

Fig. 4. Optical micrographs of the eutectic Si particles in the Al-7 wt% Si alloy subjected to different thermal treatments and processing: a) as-cast C sample+ ECAP-4p-B_C; b) annealed and quenched Q sample + ECAP; c) annealed and furnace cooled S sample +ECAP; d) C sample + HPT-N=5; 6 GPa; e) Q sample + HPT; f) S sample + HPT. HPTed samples were analyzed on the periphery disc zone (~0.8 r).

Fig. 5. a) and c) Secondary and b) and d) backscattered electron micrographs of the as-cast Al-7 wt% Si alloy (C sample) processed by a) and b) ECAP-4 passes-B_C; c) and d) HPT-N=5; 6 GPa.

Fig. 6. a) and c) Secondary and b) and d) backscattered electron micrographs of the microstructure of the annealed and quenched Al-7 wt% Si alloy (Q samples) processed by a) and b) ECAP-4 passes-B_C; and c) and d) HPT-N=5; 6 GPa.

Fig. 7. a) and c) Secondary and b) and d) backscattered electron micrographs of the microstructure of the annealed and slow cooled Al-7 wt% Si alloy (S samples) processed by a) and b) ECAP-4 passes-B_C; and c) and d) HPT-N=5; 6 GPa.

Fig. 8. Backscattered electron micrographs showing HPTed Al-7 wt% Si microstructures around large Si particles in a) C sample; b) Q sample; d) S sample.

Table 1. Silicon concentration (weight percent) in the middle of aluminium dendritic cells for Al-7 wt% Si alloy samples, as a function of different thermal treatments.

Sample	**Si (wt%)**
As-cast (C)	1.6 ± 0.2
540 ºC-20 h + quenching (Q)	1.1 ± 0.2
540 ºC-20 h + slow cooling (S)	0.7 ± 0.1

Table 2. Average (sub)grain size on the primary Al dendrite cells of the processed samples.

Starting conditions	ECAP-4Passes (μm)	HPT (N=5; 6 GPa) (μm)
As-cast (C)	0.3	0.2/0.5*
540 ºC-20 h + water quenching (Q)	0.4	0.2
540 ºC-20 h + slow cooling (S)	0.8	0.4

* Bimodal microstructure with coarse grains near large eutectic Si particles, and fine grains where deformation-induced Si precipitates were observed.

Table 3. Vickers microhardness (HV) measurements of the starting and processed Al-7 wt% Si samples.

Starting conditions	HV-Initial (1 kg; 15 s)	HV-ECAP-4p-B_C (1 kg; 15 s)	HV-ECAP-4p-B_C (10 g; 15 s)	HV-HPT (N=5; 6 GPa) (1 kg;15 s)
As-cast (C)	44 ± 2	69 ± 1	72 ± 3	77 ± 2
540 ºC-20 h + water quenching (Q)	42 ±1	73 ± 2	62 ± 2	**84** ± 1
540 ºC-20 h + slow cooling (S)	34 ± 2	51 ± 2	46 ± 2	64 ± 2

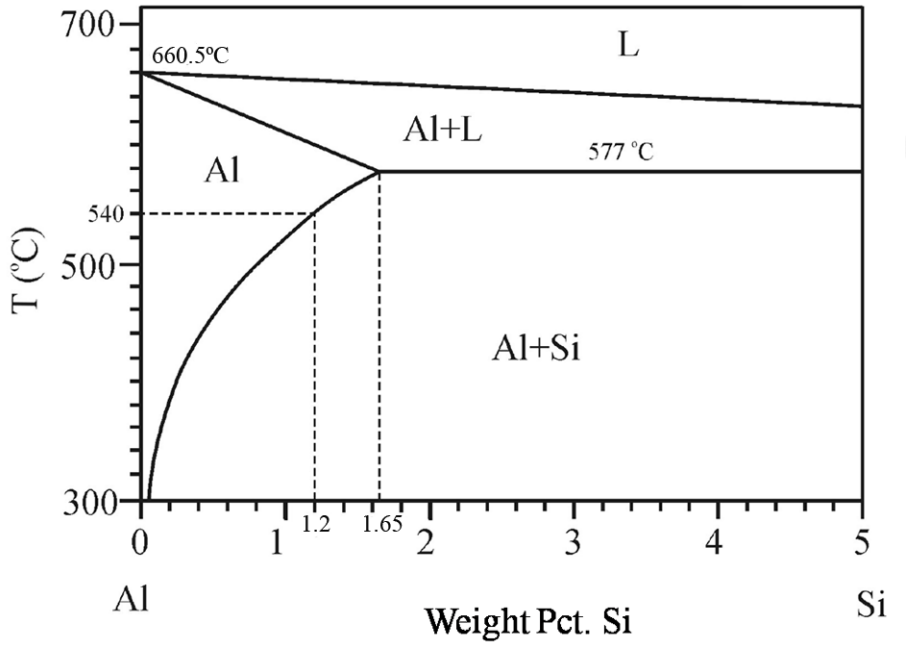

Fig. 1. Detail of the Al-Si phase diagram from 0 to 5wt%Si.

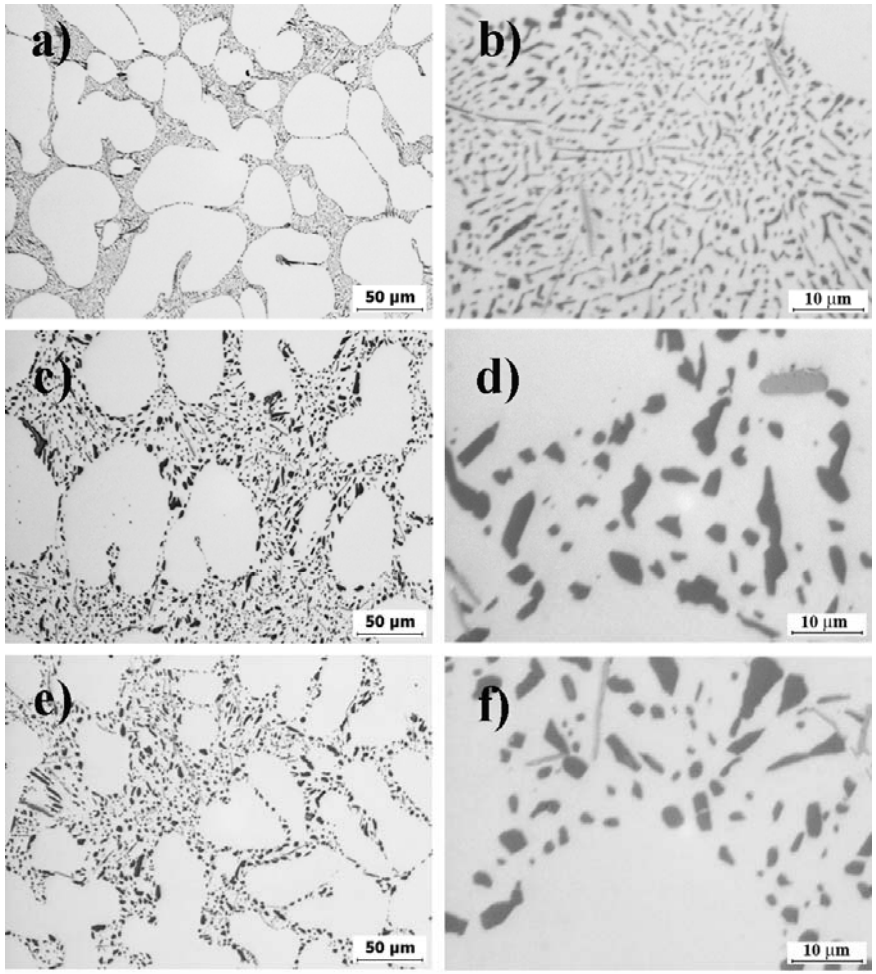

Fig. 2. Optical micrographs at two magnifications showing primary Al dendritic cells and eutectic Si particles in the Al-7 wt% Si alloy subjected to different thermal treatments: a) and b) as-cast C sample; c) and d) annealed and quenched Q sample; e) and f) annealed and furnace cooled S sample.

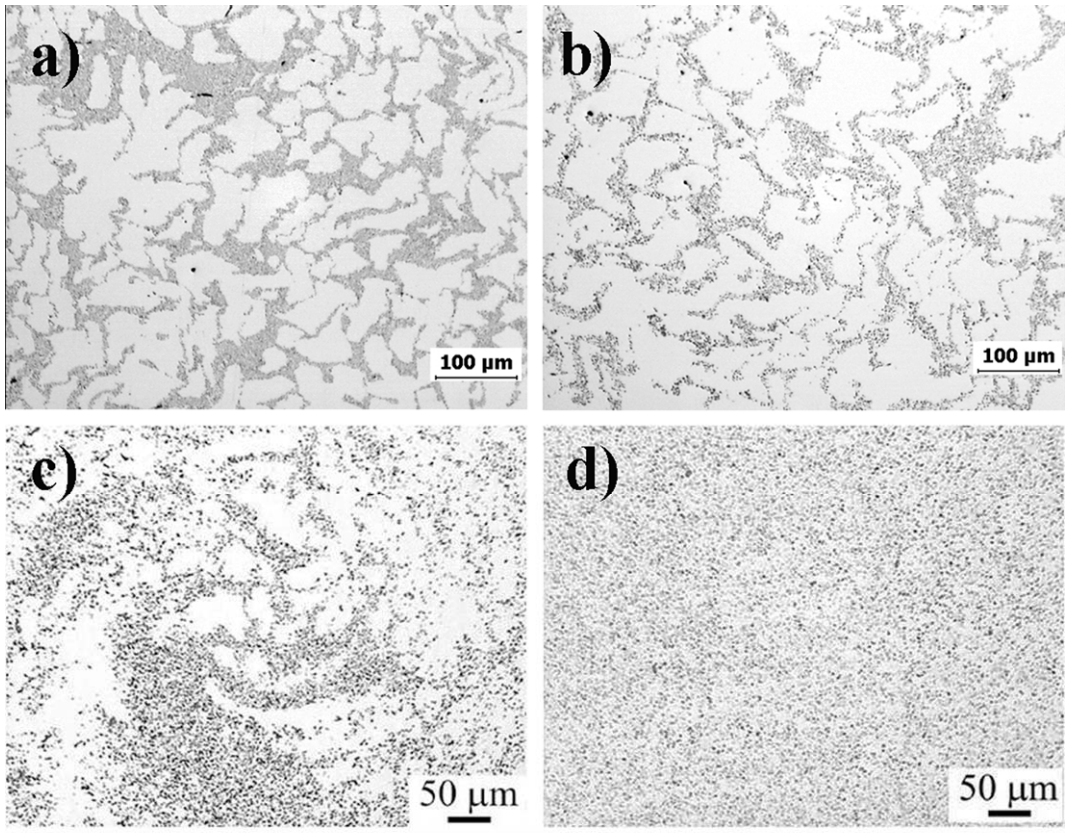

Fig. 3. Optical micrographs of the as-cast Al-7 wt% Si alloy (C sample) processed by: a) 4 ECAP passes and b) 8 ECAP passes by route B_C; c) HPT-N=5 and 6 GPa on the central disc zone; and d) HPT-N=5 and 6 GPa on the periphery disc zone.

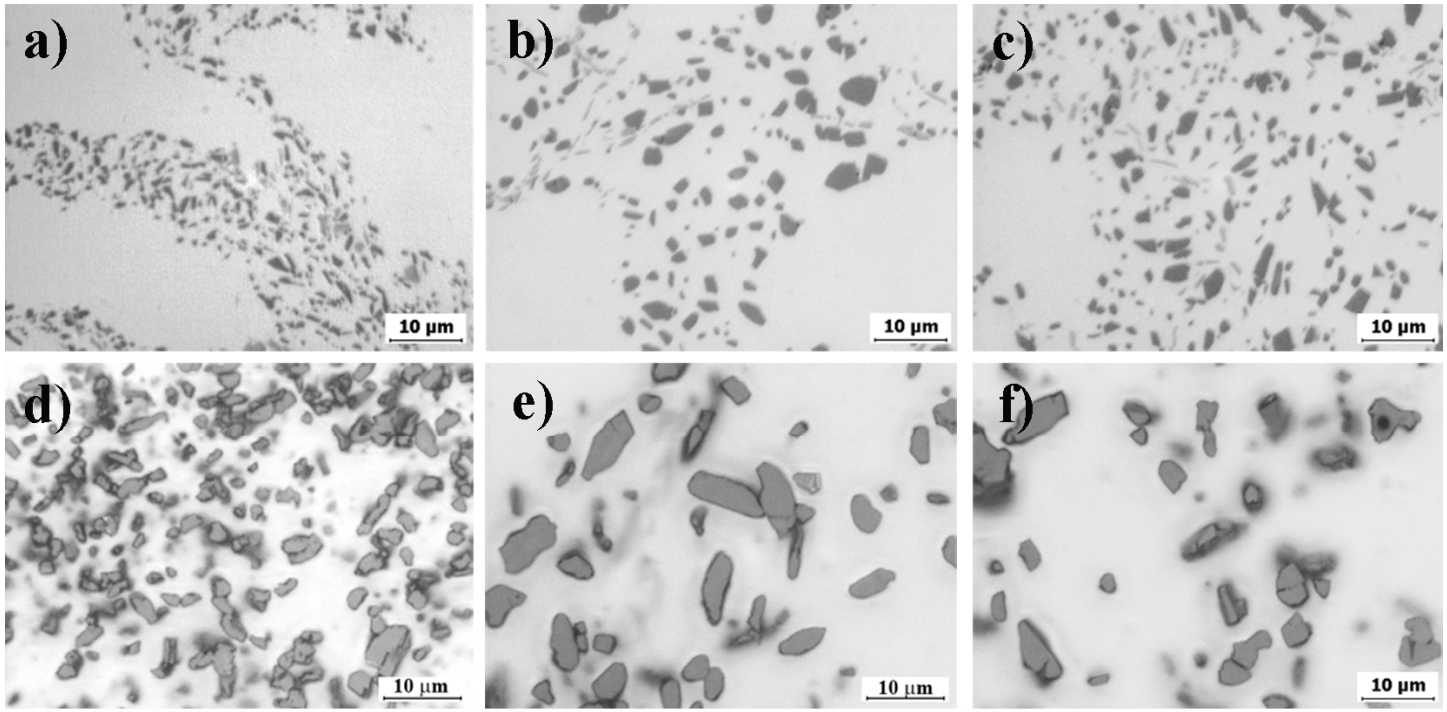

Fig. 4. Optical micrographs of the eutectic Si particles in the Al-7 wt% Si alloy subjected to different thermal treatments and processing: a) as-cast C sample+ ECAP-4p-B_C; b) annealed and quenched Q sample + ECAP; c) annealed and furnace cooled S sample +ECAP; d) C sample + HPT-N=5; 6 GPa; e) Q sample + HPT; f) S sample + HPT. HPTed samples were analyzed on the periphery disc zone (0.8 r).

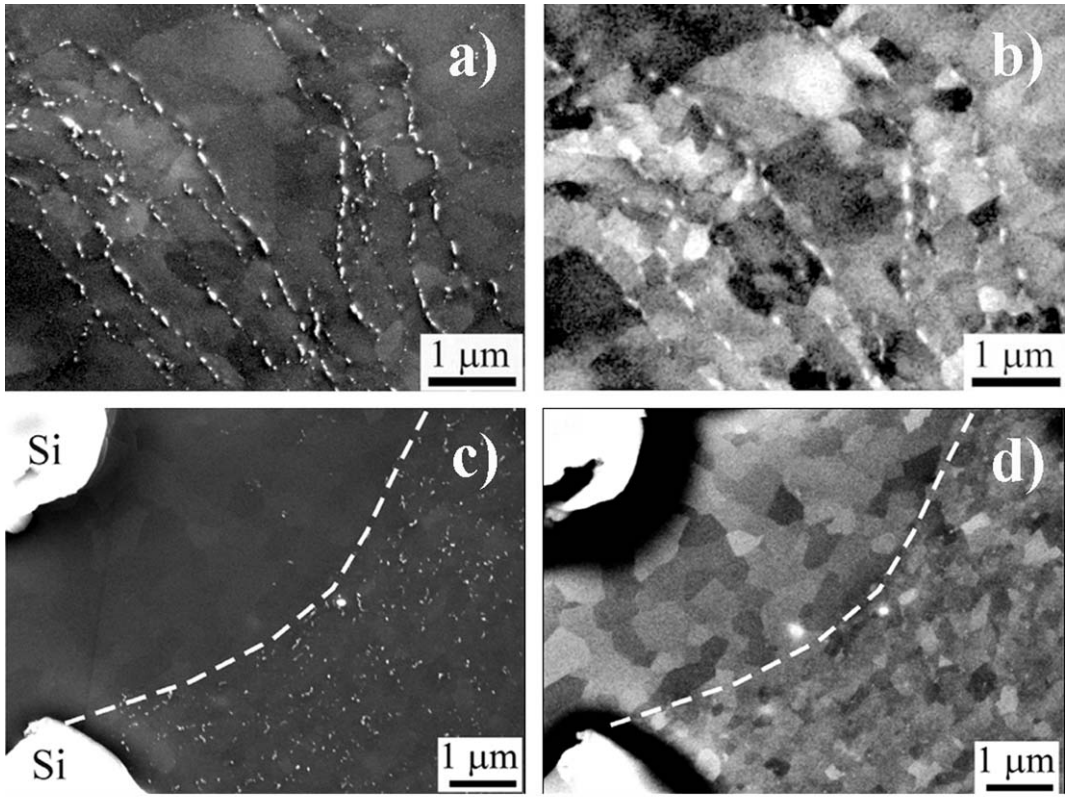

Fig. 5. a) and c) Secondary and b) and d) backscattered electron micrographs of the as-cast Al-7 wt% Si alloy (C sample) processed by a) and b) ECAP-4 passes-B_C; c) and d) HPT-N=5; 6 GPa.

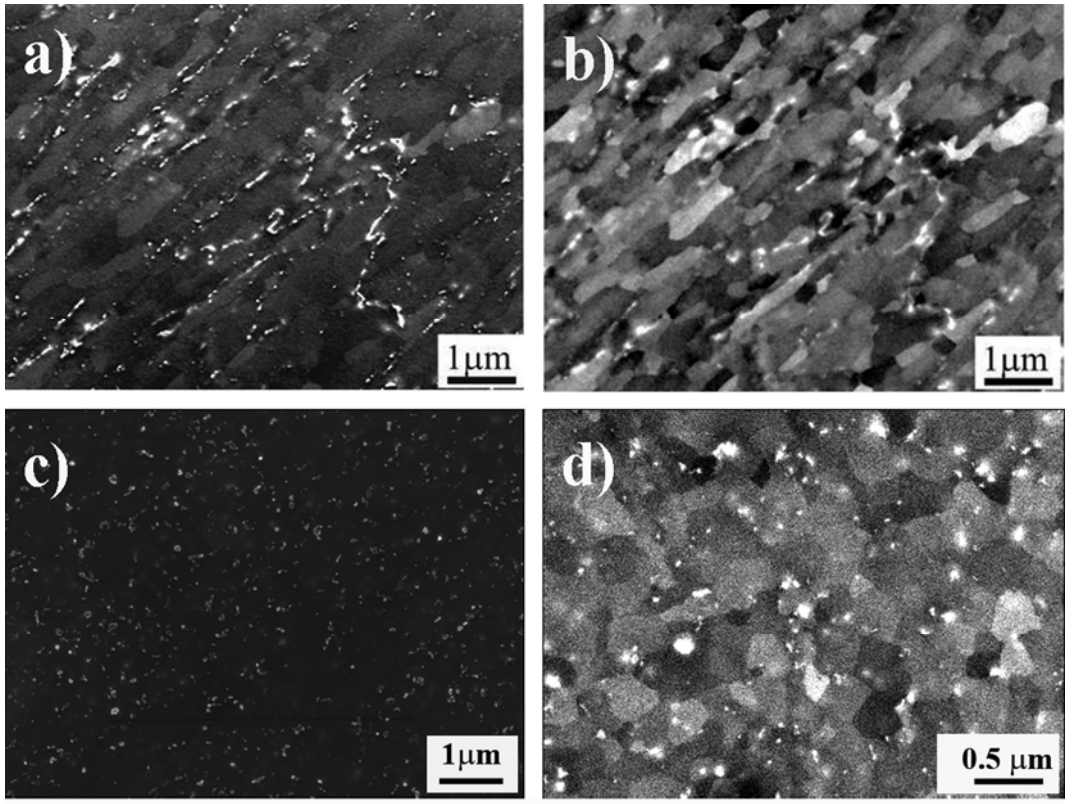

Fig. 6. a) and c) Secondary and b) and d) backscattered electron micrographs of the microstructure of the annealed and quenched Al-7 wt% Si alloy (Q samples) processed by a) and b) ECAP-4 passes-B_C; and c) and d) HPT-N=5; 6 GPa.

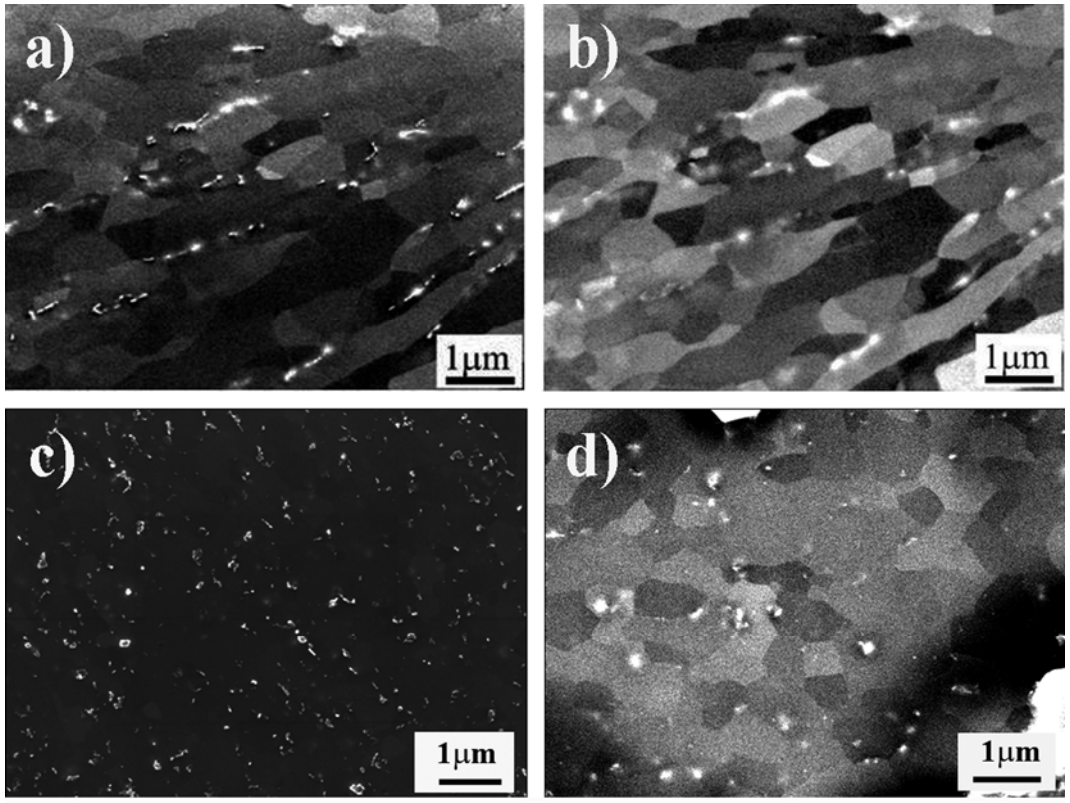

Fig. 7. a) and c) Secondary and b) and d) backscattered electron micrographs of the microstructure of the annealed and slow cooled Al-7 wt% Si alloy (S samples) processed by a) and b) ECAP-4 passes-B_C; and c) and d) HPT-N=5; 6 GPa.

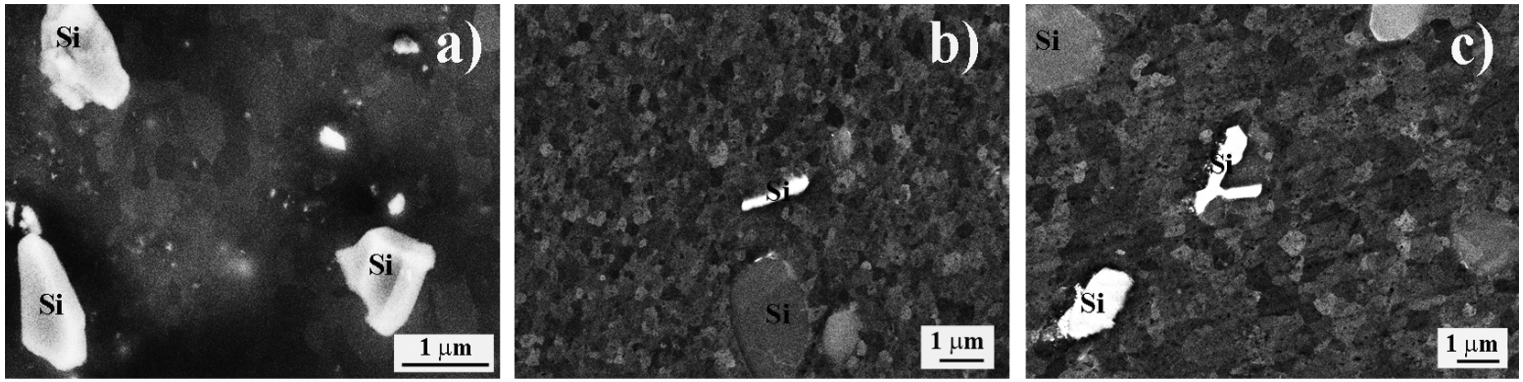

Fig. 8. Backscattered electron micrographs showing HPTed Al-7wt%Si microstructures around large Si particles in a) C sample; b) Q sample; d) S sample.